Int. J. Electrochem. Sci., 13 **(2018)** 5788 – 5797, doi: 10.20964/2018.06.20

International Journal of
ELECTROCHEMICAL
SCIENCE
www.electrochemsci.org

Bimetallic Zeolitic Imidazolate Framework-derived Porous Carbon as Efficient Bifunctional Electrocatalysts for Zn-air Battery

Zihan Meng[1,2], *Haopeng Cai*[1,*], *Haolin Tang*[2,*]

[1] School of Material Science and Engineering, Wuhan University of Technology, Wuhan, China, 430070

[2] State Key Laboratory of Advanced Technology for Materials Synthesis and Processing, Wuhan University of Technology, Wuhan, China, 430070

[*]E-mail: cai_haopeng@whut.edu.cn, thln@whut.edu.cn

Received: 27 January 2018 / *Accepted:* 21 March 2018 / *Published:* 10 May 2018

The development of low-cost and efficient oxygen reduction reaction (ORR) and oxygen evolution reaction (OER) electrocatalyst is critical for widespread application of fuel cells and metal-air batteries. Herein, hierarchically structured porous carbon bifunctional electrocatalyst is synthesized by using soft template and metal organic framework (MOF) precursor. The as-obtained electrocatalyst exhibits superior catalytic activity due to its hierarchical porous architecture as well as high surface area (1539 m^2 g^{-1}). For ORR, the prepared catalyst shows more positive activity, superior long-term stability and remarkable methanol tolerance compared with commercial Pt/C catalyst in alkaline condition. In addition, the reported catalyst also has a higher OER activity than commercial Pt/C catalyst in alkaline media. We further demonstrate that the catalyst also presents outstanding Zn-air battery performance.

Keywords: Metal organic framework, soft template, oxygen reduction reaction, oxygen evolution reaction; Zn-air battery

1. INTRODUCTION

With the rapid consumption of conventional non-renewable fossil fuels, our declining environment motivates us to develop sustainable energy conversion and storage systems such as fuel cells[1-3] and metal-air batteries[4-6]. Among various types of environment-friendly devices, Zn-air battery has been considered as promising technology owing to its high energy density, low cost, and

environmental friendliness. Oxygen electrode reactions, such as oxygen reduction reaction (ORR) and oxygen evolution reaction (OER), are critical reactions involved in the working process of these devices. Both ORR and OER have high activation barriers and normally need to be catalyzed with precious metals-based catalysts such as Pt- and Ru/Ir-based catalysts[7, 8]. Apart from their relatively low stability in the catalytic process, these precious metal based catalyst also suffer from their high cost. Thus, development of earth-abundant ORR/OER catalysts with comparable electrocatalytic activity to their noble-metal counterparts is essential for the development Zn-air battery.

Up to now, numerous studies have been devoted to develop earth-abundant materials as electrocatalysts[9-12]. Transition metal-nitrogen-carbon (M-N-C) electrocatalyst has attracted increasing interest due to its low cost, superior catalytic activity and chemical stability[13-15]. In particular, M-N-C based on carbonized metal-organic framework (MOF) is shown to possess high specific surface area, controllable pore structure, and tunable composition, which offer an opportunity to acquire superior bifunctional electrocatalyst[16, 17]. However, most MOF precursor is microporous (pore size<2 nm), which leads to its large pore volume and high surface area, but the small pore size often results in a drastic fusion and aggregation of nanoparticles, giving rise to reducing the number of active sites and blocking the passway of mass transfer in high temperature pyrolysis process[18, 19]. In addition, mesopore structure reduces diffusion path for oxygen as well as active species and offers large interfacial area for reaction, rapid pathway for charge transport.[20, 21] Furthermore, the usually tedious post-treatment processes such as durable hot acid leaching and/or repetitive high temperature pyrolysis observably increase the cost of its production[22, 23]. Therefore, it is urgent to design electrocatalysts with hierarchically pore structure and high specific surface area simultaneously by a simple and low-cost way.

Zeolitic imidazolate framework (ZIF) have been considered as low-cost precursors for oxygen electrocatalysts[24]. Herein, we report a novel and facile synthesis of a series of high performance M-N-C bifunctional electrocatalysts by high temperature pyrolysis of bimetallic ZIF self-assembled into structure-directing agent (P123) under aqueous medium. The porous feature of M-N-C catalyst was finely controlled by using the structure-directing agent and sacrificial Zn species. The optimal N-M-C catalyst identified herein possessed a large surface area (1539 $m^2 g^{-1}$) with hierarchical morphology that allows for a high density of catalytic active site as well as efficient transport process, and thus exhibits excellent oxygen catalytic activity. More importantly, the catalyst also shows competitive Zn-air battery performance.

2. EXPERIMENTAL SECTION

Materials and chemicals. $Co(NO_3)_2 \cdot 6H_2O$, $Zn(NO_3)_2 \cdot 6H_2O$, and $Zn(AC)_2 \cdot 2H_2O$ were purchased from Sinopharm Chemical Reagent Co., Ltd., China. 2-methylimidazole (mIm, 98%), acetylene black, and pol (vinylidene fluride) (PVDF) were purchased from Aladdin Reagent Co., Ltd. Pluronic P123 (Mw = 5800), Pt/C (20 wt%), and Zn plate were purchased from Sigma-Aldrich Co., Ltd. Nafion solution (5 wt%) was purchased from DuPont Co., Ltd.

Synthesis of ZIF materials. Typically, 0.04 mmol (0.232 g) of P123 was dissolved in 48 mL deionized water to form a clear solution at 40℃, a mixture of 8 ml deionized water containing 20 mmol (1.6422 g) of 2-methylimidazole was added to above solution with stirring for 8 h, then 2 mmol of transition metal nitrate [$Co(NO_3)_2 \cdot 6H_2O$ or $Zn(NO_3)_2 \cdot 6H_2O$ or their mixture] dissolved in 8 mL deionized water was poured into above solution and stirred for another 10 min. The reaction mixture was transferred to a 100 mL Teflon-lined stainless steel autoclave and maintained at 40℃ for 24 h. The solid products were centrifuged and washed with deionized water and ethanol for three times and finally dried at 60℃ in vacuum.

Synthesis of carbon-based electrocatalysts. The powders of ZIF materials were placed in a tube furnace under N_2 atmosphere and heated to 400℃ with a heating rate of 1℃ min^{-1} for 1.5 h, subsequently the temperature was ramped to 600℃ with a heating rate of 1℃ min^{-1}, then increased to 900℃ with a heating rate of 5℃ min^{-1} and maintained for another 3 h. The carbon-based electrocatalysts prepared from ZIF were denoted as HC-xCo(100-x)Zn, where x was defined as the molar percentage of Co/(Zn + Co) in precursor.

General Characterizations. Transmission electron microscopy (TEM) and elemental mapping images were obtained on a JEOL JEM-2100F microscope. N_2 adsorption-desorption measurements were performed with a Micromeritics Tristar II 3020 analyzer at 77 K in a N_2 atmosphere. The specific surface area (S_{BET}) was calculated by the Brunauer-Emmett-Teller (BET) method and the pore-size distribution was obtained by the Barret-Joyner-Halenda (BJH) model. *Electrochemical measurements.* All the ORR and OER electrochemical measurements were performed with a CHI 660E electrochemical workstation using a standard three-electrode cell with a reversible hydrogen electrode (RHE) as reference electrode, a Pt plate as counter electrode, and a catalyst film coated rotating disk electrode as working electrode. The catalysts were prepared by ultrasonically dispersing 5 mg of the catalyst powder with the mixture of 800 μL of isopropanol, 200 μL of deionized water and 20 μL of 5% Nafion solution for 20 min to form homogeneous catalyst inks.

Linear sweep voltammetry (LSV) measurement was recorded over the potential range of 0 to 1.2 V with a scan rate of 5 mV s^{-1}. The stability and CH_3OH (3M) tolerance tests of the catalyst were evaluated by current vs. time (i-t) chronoamperometric response during a constant potential of 0.6 V at a rotation rate of 1600 rpm.

To further calculate the average electron transfer number (n), the Koutecky-Levich (K-L) equation is given as follow:

$$\frac{1}{J} = \frac{1}{J_L} + \frac{1}{J_K} = \frac{1}{B\omega^{\frac{1}{2}}} + \frac{1}{J_K}$$

$$B = 0.2nFC_0{D_0}^{2/3}V^{-1/6}$$

where J is the measured current density, J_K and J_L are the kinetic and limiting current densities, respectively, ω is the rotating speed, n is the electron transfer number, F is the Faraday constant (96485 C mol^{-1}), C_0 is the bulk concentration of O_2 (1.2×10^{-6} mol cm^{-3}), D_0 is the diffusion coefficient of O_2 (1.9×10^{-5} cm^2 s^{-1}), V is the kinematic viscosity of the electrolyte (0.01 cm^2 s^{-1}).

The linear sweep voltammetry measurements for OER were recorded over the potential range of 1.2 to 2 V at 1600 rpm in O_2-saturated 0.1 M KOH with a scan rate of 5 mV s^{-1}.

Zn-air battery tests. For the Zn-air battery tests, the air electrode was prepared by uniformly coating the as-prepared electrocatalyst (HC-5Co95Zn and Pt/C) ink onto hydrophobic carbon paper, whereas a piece of polished Zinc plate was used as anode and 6 M KOH containing 0.2 M zinc acetate was used as electrolyte. To prepare carbon paper supported electrode with a catalyst loading of 0.1 mg cm^{-2}, 80% catalyst, 10% acetylene black, and 10% pol (vinylidene fluride) (PVDF) were mixed in N-methyl-2-pyrrolidone (NMP) to form a homogeneous slurry and dried at 60 ℃ for 6 h.

3. RESULTS AND DISCUSSION

The ZIF-based hierarchically porous bifunctional electrocatalyst is fabricated by a three-step process. Firstly, P123 micelles were dissolved in aqueous medium and 2-methylimidazole were self-assembled onto the micelles through hydrogen bond. Next, ZIF crystal arrays were grown on the micelles after adding transition metal nitrate. Finally, the ZIF arrays were collected and a carbonization treatment was performed to remove soft template and acquire M-N-C material. The choice of aqueous solution rather than toxic and flammable organic solvent makes the preparation of ZIF precursors environment-friendly but to obtain equivalently ZIF material without using a great excess of linker or complex synthetic routes.

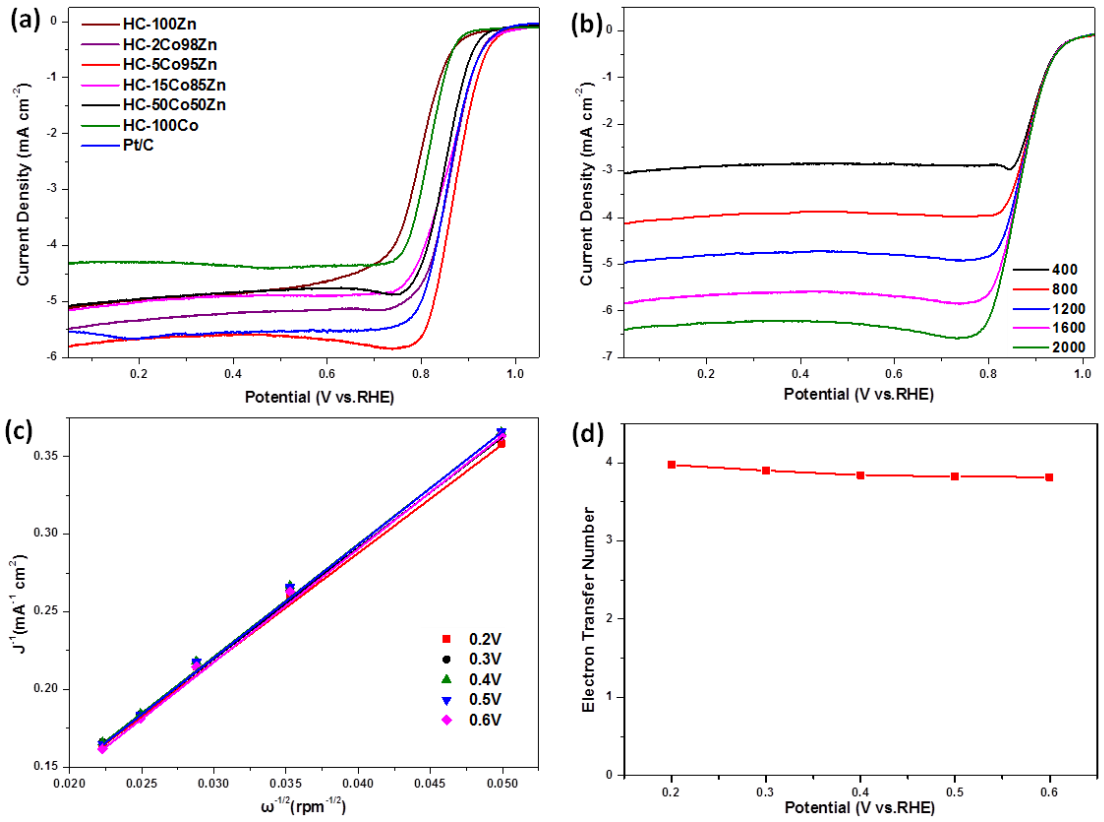

Figure 1. LSV curves of the HC-xCo(100-x)Zn and Pt/C for ORR in O_2-saturated 0.1 M KOH at 1600 rpm (a). LSV curves of HC-5Co95Zn collected at various rotation speeds in O_2-saturated 0.1 M KOH solution (b). Koutecky–Levich (K-L) polts of HC-5Co95Zn electrode at different

potentials (c). The calculated ORR electron transfer number of HC-5Co95Zn at different potentials (d).

A robust catalyst that is applicable in Zn-air battery should be catalytic active in both ORR and OER. Here, the ORR activity of HC-xCo(100-x)Zn was first evaluated by linear sweep voltammetry (LSV) measurements, and the catalytic activity is characterized by the onset potential (E_{onset}) and half-wave potential ($E_{1/2}$). At a rotation rate of 1600 rpm (Figure 1a), HC-100Co and HC-100Zn show limited activities with half-wave potentials of 0.82 and 0.80 V, respectively. Among all the catalysts, HC-5Co95Zn exhibits excellent ORR activity (E_o=0.96 V, $E_{1/2}$=0.88 V), which is superior to Pt/C (E_o=0.95 V, $E_{1/2}$=0.86 V) and most previously reported non-precious ORR catalysts[25, 26]. To further investigate the ORR performance of the synthesized HC-5Co95Zn, LSV were performed with various rotating speeds from 400 to 2000 rpm (Figure 1b). The K-L plots and the number of electrons transfer (n) were obtained to better understand the mechanism during ORR. The K-L plots (Figure 1c) resulted in nearly parallel fitting lines reveals that HC-5Co95Zn acts up to the first-order reaction kinetics toward the concentration of O_2 from 0.2 to 0.6 V. The calculated electron transfer numbers (Figure 1d) for HC-5Co95Zn is in the range of 3.82-3.97, which is close to those of Pt/C [27], suggesting the ORR with HC-5Co95Zn catalyzed is a quasi-four-electron process.

In addition to the activity, the long-term stability is also essential for a high-performance ORR catalyst. The stability of HC-5Co95Zn and Pt/C was investigated by 50000 s current vs. time (i-t) chronoamperometric response in 0.1 M KOH solution. Figure 2a shows that Pt/C exhibited 25.0% loss of the current density after 50000 s, whereas HC-5Co95Zn exhibits only 10.4% decrease, demonstrating that HC-5Co95Zn is more stable than Pt/C toward ORR in alkaline medium. The methanol tolerance of HC-5Co95Zn and Pt/C was further assessed. As shown in Figure 2b, HC-5Co95Zn exhibits a negligible variation compared with Pt/C of the chronoamperometric curve after introduction of 3 M methanol at 500 s, the results here suggest that HC-5Co95Zn has excellent immunity toward methanol crossover, making it a promising catalyst for energy conversion devices such as direct methanol fuel cells.

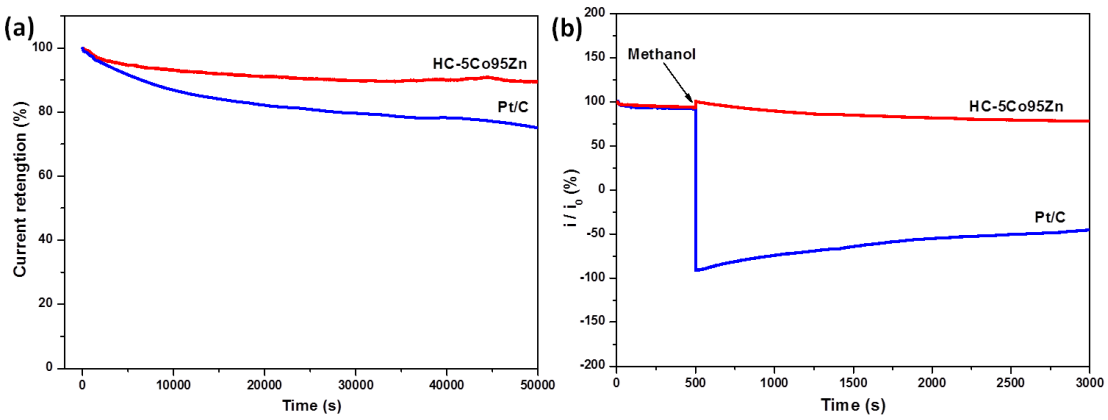

Figure 2. Chronoamperometric response of HC-5Co95Zn and Pt/C in O_2-saturated 0.1 M KOH (a). Chronoamperometric response of HC-5Co95Zn and Pt/C on addition of 3 M methanol in O_2-saturated 0.1 M KOH (b).

Since oxygen evolution reaction is also involved in the electrode process of metal-air battery, the OER performance of the catalysts was also investigated. The electrocatalytic activity of catalysts towards OER was characterized by the LSV in 0.1 M KOH. The OER catalytic activity is evaluated with the operating potential at a current density of 10 mA cm^{-2} ($E_{j=10}$), which is a critical metric applicable to OER tests[28]. As shown in Figure 3a, HC-5Co95Zn displayed a current density of 10 mA cm^{-2} at 1.70 V, the potential is smaller than Pt/C and electrocatalysts with different molar ratio of Co/Zn from HC-5Co95Zn, even comparable with the state-of-art RuO_2 electrocatalyst[29, 30], indicating an improved catalytic activity in HC-5Co95Zn for OER. The overall electrocatalytic activity of the catalysts for reversible ORR and OER are evaluated through the potential gap (ΔE) (Figure 3b) between the half-wave potential ($E_{1/2}$) for ORR and $E_{j=10}$ for OER ($\Delta E = E_{j=10} - E_{1/2}$)[31]. Consequently, HC-5Co95Zn displays the lowest ΔE of 0.82 V among electrocatalysts with different molar ratio of Co/Zn from HC-5Co95Zn and Pt/C. The results outperform major non-precious metal bifunctional electrocatalyst (Table 1) and demonstrate that HC-5Co95Zn is a promising candidate for bifunctional catalyst.

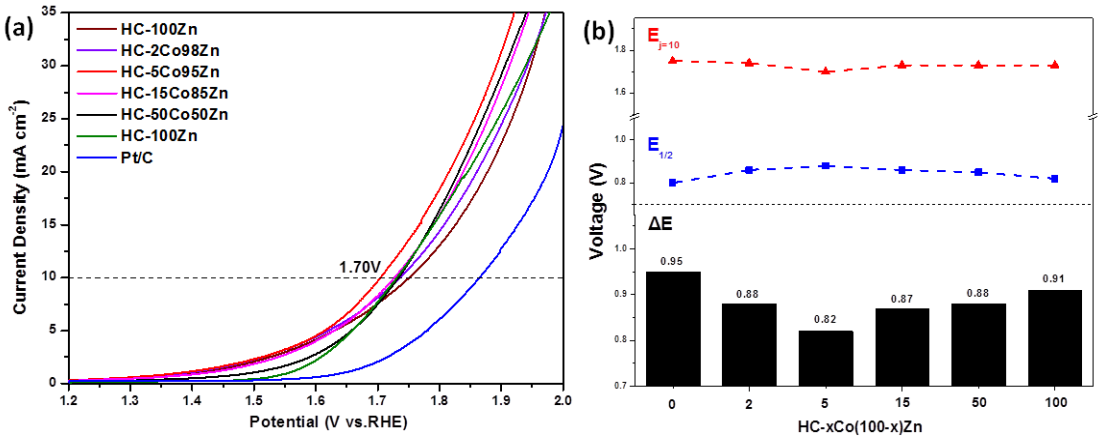

Figure 3. LSV curves of the HC-xCo(100-x)Zn and Pt/C for OER in O_2-saturated 0.1 M KOH solution at 1600 rpm (a). The potential with current density of 10 mA cm^{-2} ($E_{j=10}$), the half-wave potential ($E_{1/2}$), and potential gap ΔE of HC-xCo(100-x)Zn (b).

Table 1. Comparison of ORR and OER parameters over various non-precious metal electrocatalysts in alkaline media

sample	$E_{1/2}$ (V vs. RHE)	$E_{j=10}$ (V vs. RHE)	ΔE (V vs. RHE)	Ref.
HC-5Co95Zn	0.88	1.70	0.82	This work
NiO/CoN PINWs	0.68	1.52	0.84	[9]
NMC/Co@CNTs	0.79	1.73	0.94	[15]
Co4N/CNW/CC	0.80	1.53	0.73	[17]
Co3O4/ NBGHSs	0.86	1.72	0.84	[29]
NPMC-1000	0.86	1.80	0.94	[30]
CoS2(400)/N,S-GO	0.79	1.62	0.83	[31]

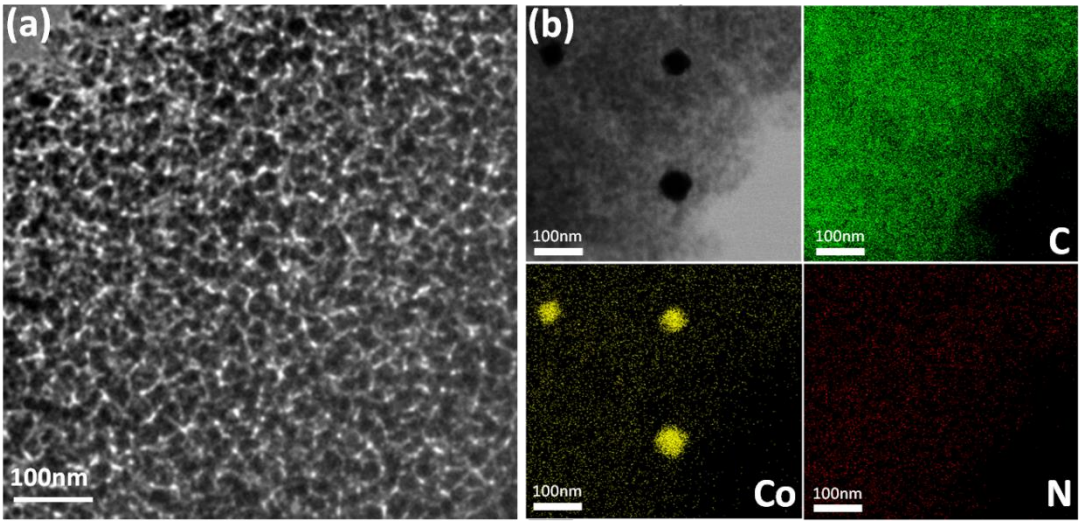

Figure 4. TEM images(a) and Elemental mapping (b) of HC-5Co95Zn.

To gain deeper insight into the morphological characteristics of the sample, transmission electron microscopy (TEM) measurment was conducted. As revealed by TEM (Figure 4a), well-defined mesoporous structure with the parameter of around 20 nm can be observed clearly from HC-5Co95Zn. Element mapping images (Figure 4b) confirm the uniform distribution of C, N, and highly dispersed Co nanoparticles.

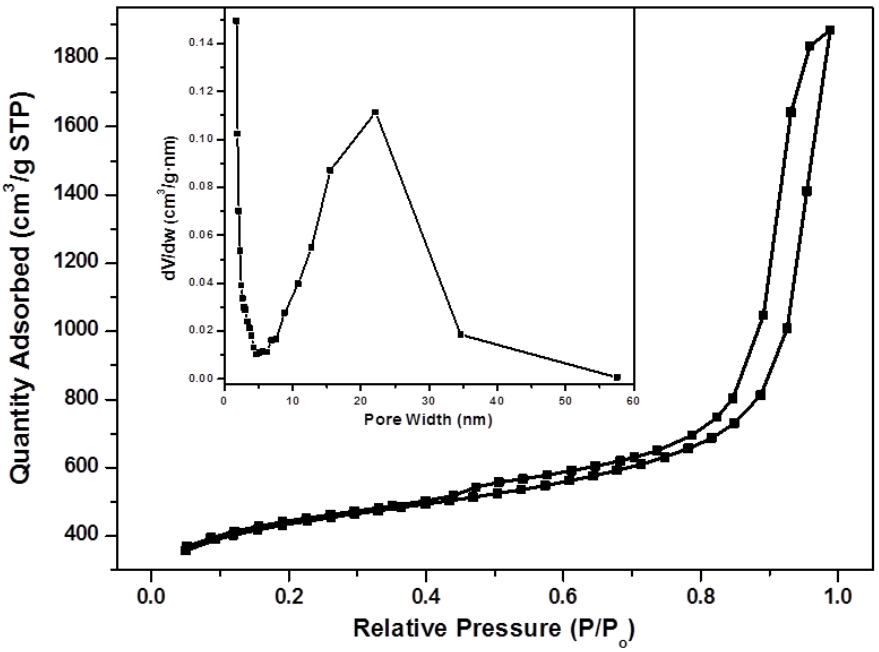

Figure 5. Nitrogen adsorption-desorption isotherms of HC-5Co95Zn and the inset is its corresponding pore-size distribution.

To further understand the excellent ORR and OER performance of HC-5Co95Zn and prove the formation of hierarchically pore structure, N_2 adsorption-desorption measurements were performed. Typical IV-type isotherm with hysteresis loops[32] is observed for HC-5Co95Zn (Figure 5), indicating the presence of mesopore. The pore-size distribution of HC-5Co95Zn simulated from N_2 adsorption-desorption isotherms shows that HC-5Co95Zn is rich in micropore and mesopore. The surface area (S_{BET}) of HC-5Co95Zn (Table 2) are calculated by the Brunauer-Emmett-Teller (BET) method, which exceeding most of carbon-based materials derived from MOF.[33, 34]

Table 2. Structural parameters of HC-5Co95Zn

sample	S_{BET} (m^2 g^{-1})	t-Plot micropore area (m^2 g^{-1})	t-Plot micropore volume (cm^3 g^{-1})	Pore volume (cm^3 g^{-1})
HC-5Co95Zn	1539	688	0.298	2.913

From the analysis above, the superior activity of HC-5Co95Zn may be attributed to synergistic effect of its unique features: (1) the hierarchical pore structure rather than single pore structure provides short diffusion channels for the penetration and transportation of O_2 and ions, thus enable fast mass exchanges during the reaction process; (2) the finely dispersive Co and N species as well as high surface area (1539 m^2 g^{-1}) afford a full exposure for active sites that ensure they can interact closely with O_2;

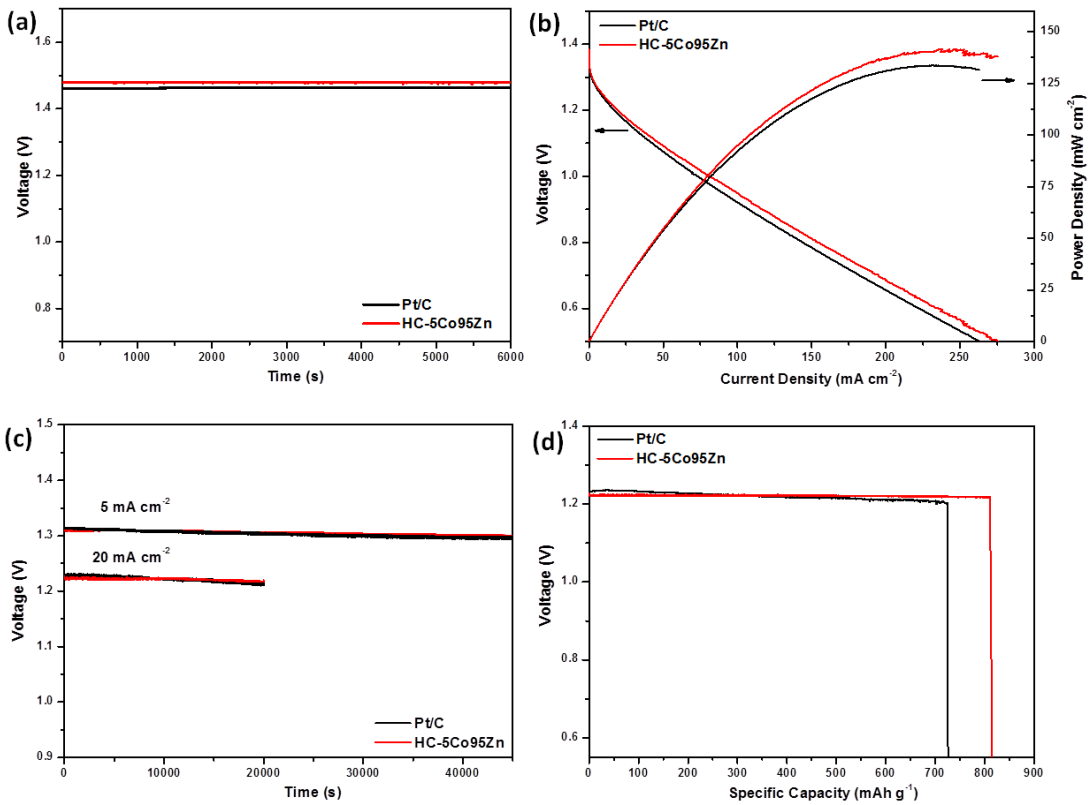

Figure 6. Open circle potentials (a), polarization curves and power densities (b) of primary Zn-air batteries using HC-5Co95Zn and Pt/C. Discharge curves of the Zn-air batteries using HC-5Co95Zn and Pt/C at various current densities (c). Specific capacity of primary Zn-air batteries using HC-5Co95Zn and Pt/C (d).

Furthermore, primary Zn-air battery was assembled with HC-5Co95Zn and its cell performance was also evaluated. The primary Zn-air battery with HC-5Co95Zn worked stably for more than 6000 s at a high open-circuit potential of 1.48 V (Figure 6a) which outperforms that of Pt/C (1.46 V), suggesting a good catalytic performance of HC-5Co95Zn. Figure 6b shows the polarization curves and power densities of HC-5Co95Zn and Pt/C. HC-5Co95Zn shows a high power density of 142 mW cm^{-2} which exceeded that of Pt/C (133 mW cm^{-2}). The galvanostatic discharge polarization curves (Figure 6c) clearly revealed the battery performance of HC-5Co95Zn exhibited little activity decay with high potential of 1.31 and 1.22 V at the discharge current densities of 5 and 20 mA cm^{-2}. The excellent discharge performance of HC-5Co95Zn was comparable to that of commercial Pt/C catalyst. The specific capacity of Zn-air battery composed of HC-5Co95Zn is measured to be 815 mA h g^{-1} (Figure 6d) at the discharge current densities of 20 mA cm^{-2} which is slightly higher than that of Pt/C (715 mA h g^{-1}). The superior performance of the Zn-air battery with HC-5Co95Zn consistent with its outstanding electrocatalytic activity as well as its hierarchical pore structure that facilitating efficient diffusion of O_2 gas and electrolyte towards the active sites.

4. CONCLUSION

In summary, ZIF-derived hierarchically porous bifunctional catalysts were successfully synthesized by a low-cost and environment-friendly preparation process. The high temperature treatment of ZIF precursor offers abundant micropore and the mesopores are developed by controlled patterning of ZIF precursor on P123 micelles. The unique hierarchical porous architecture of HC-5Co95Zn catalyst as well as its compositional features endows the catalyst with excellent activity for both ORR and OER. As a result, Zn-air battery fabricated with HC-5Co95Zn also exhibits outstanding performance that is superior to those for Pt/C catalyst. This work not only demonstrates a highly promising electrocatalyst for energy conversion and storage devices but may also offer a novel viewpoint for the design and preparation of hierarchically porous carbon materials for a variety of applications. This work may offer a novel viewpoint for the design and preparation of hierarchically porous electrocatalysts derived from MOF materials for energy conversion and storage devices.

References

1. J. Luo, A.H. Jensen, N.R. Brooks, J. Sniekers, M. Knipper, D. Aili, Q. Li, B. Vanroy, M. Wübbenhorst, F. Yan, *Energy & Environmental Science* 8 (2015) 1276-1291.
2. J. Luo, O. Conrad, I.F.J. Vankelecom, *Journal of Materials Chemistry* A 1 (2013) 2238-2247.
3. A. Brouzgou, S. Song, Z.X. Liang, P. Tsiakaras, *Catalysts* 6 (2016) 159.
4. Z. Cui, L. Li, A. Manthiram, J.B. Goodenough, *J Am Chem Soc* 137 (2015) 7278-7281.
5. P. Yin, T. Yao, Y. Wu, L. Zheng, Y. Lin, W. Liu, H. Ju, J. Zhu, X. Hong, Z. Deng, *Angewandte Chemie* 55 (2016) 10800.
6. M. Zeng, Y. Liu, F. Zhao, K. Nie, N. Han, X. Wang, W. Huang, X. Song, J. Zhong, Y. Li, *Advanced*

Functional Materials 26 (2016) 4397-4404.
7. J. Li, H. Tang, R. Chen, D. Liu, Z. Xie, M. Pan, S.P. Jiang, *Journal of Materials Chemistry* A 3 (2015) 15001-15007.
8. T. Reier, M. Oezaslan, P. Strasser, *ACS Catalysis* 2 (2012) 1765-1772.
9. J. Yin, Y. Li, F. Lv, Q. Fan, Y.Q. Zhao, Q. Zhang, W. Wang, F. Cheng, P. Xi, S. Guo, *ACS Nano* 11 (2017) 2275-2283.
10. H. Wu, L. Shi, J. Lei, D. Liu, D. Qu, Z. Xie, X. Du, P. Yang, X. Hu, J. Li, *Journal of Power Sources* 323 (2016) 90-96.
11. Y. Hua, T. Jiang, K. Wang, M. Wu, S. Song, Y. Wang, P. Tsiakaras, *Applied Catalysis* B *Environmental* 194 (2016) 202-208.
12. L. Cao, Z. Lin, J. Huang, X. Yu, X. Wu, B. Zhang, Y. Zhan, F. Xie, W. Zhang, J. Chen, *International Journal of Hydrogen Energy* 42 (2017) 876-885.
13. P. Cai, S. Ci, E. Zhang, P. Shao, C. Cao, Z. Wen, *Electrochimica Acta* 220 (2016) 354-362.
14. R. Wang, J. Li, S. Cai, Y. Zeng, H. Zhang, H. Cai, H. Tang, *Chempluschem* 81 (2016) 646-651.
15. S. Cai, R. Wang, W. Guo, H. Tang, *Langmuir* 34 (2018) 1992-1998.
16. B.Y. Xia, Y. Yan, N. Li, H.B. Wu, X.W. Lou, X. Wang, *Nature Energy* 1 (2016) 15006.
17. F. Meng, H. Zhong, D. Bao, J. Yan, X. Zhang, *J Am Chem Soc* 138 (2016) 10226-10231.
18. W. Zhang, Z.Y. Wu, H.L. Jiang, S.H. Yu, *J Am Chem Soc* 136 (2014) 14385-14388.
19. Z. Yao, H. Nie, Z. Yang, X. Zhou, Z. Liu, S. Huang, *Chem Commun (Camb)* 48 (2012) 1027-1029.
20. S. Wang, L. Zhang, Z. Xia, A. Roy, D.W. Chang, J.B. Baek, L. Dai, *Angewandte Chemie International Edition* 124 (2012) 4285-4288.
21. H. Tang, Y. Zeng, D. Liu, D. Qu, J. Luo, K. Binnemans, D.E. De Vos, J. Fransaer, D. Qu, S.-G. Sun, *Nano Energy* 26 (2016) 131-138.
22. Y.Z. Chen, C. Wang, Z.Y. Wu, Y. Xiong, Q. Xu, S.H. Yu, H.L. Jiang, *Adv Mater* 27 (2015) 5010-5016.
23. N. Ranjbar Sahraie, J.P. Paraknowitsch, C. Gobel, A. Thomas, P. Strasser, *J Am Chem Soc* 136 (2014) 14486-14497.
24. J. Wei, Y. Hu, Y. Liang, B. Kong, J. Zhang, J. Song, Q. Bao, G.P. Simon, S.P. Jiang, H. Wang, *Advanced Functional Materials* 25 (2015) 5768-5777.
25. L. Lin, Q. Zhu, A.W. Xu, *J Am Chem Soc* 136 (2014) 11027-11033.
26. T. Sun, L. Xu, S. Li, W. Chai, Y. Huang, Y. Yan, J. Chen, *Applied Catalysis B: Environmental* 193 (2016) 1-8.
27. H. Tang, S. Cai, S. Xie, Z. Wang, Y. Tong, M. Pan, X. Lu, *Advanced Science* 3 (2016) 1487–1498.
28. S.S. Shinde, C.H. Lee, A. Sami, D.H. Kim, S.U. Lee, J.H. Lee, *Acs Nano* 11 (2016).
29. Z. Jiang, Z.J. Jiang, T. Maiyalagan, A. Manthiram, *Journal of Materials Chemistry* A 4 (2016) 5877-5889.
30. J. Zhang, Z. Zhao, Z. Xia, L. Dai, *Nat Nanotechnol* 10 (2015) 444-452.
31. S. Chen, J. Duan, Y. Zheng, X. Chen, X.W. Du, M. Jaroniec, S.Z. Qiao, *Energy Storage Materials* 1 (2015) 17-24.
32. M. Pramanik, Y. Tsujimoto, V. Malgras, S.X. Dou, J.H. Kim, Y. Yamauchi, *Chemistry of Materials* 27 (2015) 9320-9324.
33. B. You, N. Jiang, M. Sheng, W.S. Drisdell, J. Yano, Y. Sun, *ACS Catalysis* 5 (2015) 7068-7076.
34. P. Zhang, F. Sun, Z. Xiang, Z. Shen, J. Yun, D. Cao, *Energy & Environmental Science* 7 (2013) 442-450